Influence of process parameters on the density and magnetic properties of laser powder bed fusion NdFeB magnets

Xavier Walls[1,2*], Rene Lam[1], Mingzhang Yang[1], Mohsen K. Keshavarz[1], Fabrice Bernier[3], Alex Ellery[2], Mihaela Vlasea[1].

[1] Multi-Scale Additive Manufacturing Laboratory, Department of Mechanical and Mechatronics Engineering, University of Waterloo, Kitchener, ON, N2G 4X8, Canada.

[2] Department of Mechanical and Aerospace Engineering, Carleton University, Ottawa, ON, K1S 5B6, Canada.

[3] Automotive and Surface Transportation Research Centre, National Research Council, Boucherville, QC, J4B 6Y4, Canada.

* Corresponding author's email address: xwallspe@uwaterloo.ca

Abstract:

The demand for high-performance NdFeB permanent magnets is rapidly increasing due to their critical role in electric vehicles, wind turbines, robotics, and advanced electronics. Traditional manufacturing methods, such as sintering and bonding, are limited in design complexity, material efficiency, and sustainability. These methods require extensive machining, generate substantial waste, and often involve hazardous processing steps. Additionally, global supply chain concerns surrounding rare earth elements have intensified the need for more sustainable, resource-efficient, and locally adaptable manufacturing approaches. Laser Powder Bed Fusion (PBF-LB) presents a promising alternative to traditional methods, enabling the production of intricate geometries optimized for magnetic performance without extensive post-processing or material loss. Moreover, PBF-LB facilitates precise microstructure control to tailor magnetic properties for specific application requirements. This study examines the influence of PBF-LB process parameters on the density and magnetic properties of 3D-printed $Nd_{7.5}Pr_{0.7}Fe_{75.4}Co_{2.5}B_{8.8}Zr_{2.6}Ti_{2.5}$ magnets. A dimensionless process mapping approach was applied to optimize energy input and minimize defect formation, enabling identification of process windows that result in high-density (95 - 99%) magnets. This work explores how key process parameters such as point distance (15 – 60 µm), layer thickness (40 and 60 µm), and laser beam diameter (70 µm, focused vs. 120 µm defocused) can be optimized. The results showed that reducing point distance to a moderate range, along with reduced layer thickness and a wider defocused beam, led to lower volumetric energy densities and improved magnetic performance. Notably, higher density alone did not always correlate with superior magnetic properties. A remanence of 0.51 T and a coercivity of 673.22 kA/m were achieved. Furthermore, the optimized parameters were successfully used to fabricate complex-shaped demonstrators, showcasing the potential of PBF-LB for producing dense, structurally sound magnetic components with intricate geometries. The results highlight PBF-LB as a competitive alternative to traditional magnet fabrication methods, offering a viable pathway for the next generation of energy-efficient and sustainable magnetic materials.

Keywords: Rare earth magnets, NdFeB, laser powder bed fusion, additive manufacturing

1. Introduction

The demand for high-performance neodymium-iron-boron (NdFeB) permanent magnets is rapidly increasing due to their critical role in electric vehicles, renewable energy systems, robotics, and advanced electronics. Sintering and bonding have been the standard manufacturing methods for this type of material [1]. While sintering is effective at producing high-density magnets with a good magnetic performance, it requires significant post-processing, and it is constrained by geometric limitations. Bonded magnets, by contrast, offer greater design flexibility but sacrifice density and magnetic properties. Recent advancements in additive manufacturing (AM) offer a promising pathway to overcome the trade-offs inherent to traditional methods, while also offering an option for a more sustainable magnet production. AM technologies allow the fabrication of near-net shape magnets, significantly reducing material waste and enabling the manufacturing of complex geometries that can improve the efficiency of electromechanical systems. Various AM methods have been investigated for printing hard magnetic materials, including binder jetting [2,3], directed energy deposition [4], fused filament fabrication [5,6], and cold spraying [7,8]. Laser powder bed fusion (PBF-LB) offers significant advantages over other AM methods by fully melting the powder, resulting in higher reported relative densities (> 90%)[9], finer resolution, and eliminating the need for post-sintering processes to remove binding agents. However, the use of PBF-LB remains challenging due to common issues such as delamination, cracking, and porosity, which often prevent the successful fabrication of dense, crack-free, and magnetically functional parts.

To address these challenges, a dimensionless process mapping strategy was implemented to optimize key process parameters: point distance, layer thickness, and laser beam focus, aiming to identify process conditions that enable the fabrication of mechanically robust, highly-dense parts with complex geometries and good magnetic properties.

2. Materials and methods

Dimensionless process mapping, combined with a temperature prediction model, was used to streamline the experimental design. In this method, process parameters including laser power, exposure time, point distance (PD), and layer thickness (LT), along with physical properties of powder materials such as density, thermal conductivity, and absorptivity are integrated into two variables: normalized energy (E*) and normalized velocity (v*), as per the established protocol [10,11]. The material used for this study was an isotropic MQP-S-11-9 powder (Magnequench Corp.) with nominal composition $Nd_{7.5}Pr_{0.7}Fe_{75.4}Co_{2.5}B_{8.8}Zr_{2.6}Ti_{2.5}$ and particle size of D_{10}, D_{50}, and D_{90} of 19 µm, 37 µm, and 58 µm, respectively. Cylindrical specimens (6 mm diameter x 10 mm height) were fabricated using a modulated beam PBF-LB system (Renishaw AM400, UK) with a reduced build volume (RBV) and analyzed via Micro X-ray computed tomography (µXCT, ZEISS Xradia 520 Versa), using a voxel size of 7 µm to evaluate relative density and internal defects. Projection data was reconstructed using Dragonfly (Object Research Systems, 2023). Samples for magnetic characterization were coated in non-conductive resin (Buehler EpoThin 2), followed by grinding to ensurine direct contact of the magnets with the magnetization measurement apparatus. Magnetic remanence (B_r) and intrinsic coercivity (H_{ci}) were measured using a Permagraph L hysteresisgraph (Magnet-Physik, Indiana, USA).

3. Results and discussion

3.1. Dimensionless process mapping and density results

The results presented in this study are built upon the parameters obtained from a previous set of experiments [12] in which a sample printed with a LT of 60 µm and a focused laser beam (star marker in Figure 1), resulted in a relatively high density of 97.99% but it exhibited poor magnetic performance (pink curve in Figure 2a). Those earlier results highlighted the need for a more comprehensive process parameter optimization. One of the main issues identified was the use of an excessively small PD (3.5 µm), resulting in localized overheating. The thermal conditions during printing likely led to evaporation or segregation of the key magnetic alloying elements, compromising its magnetic behaviour.

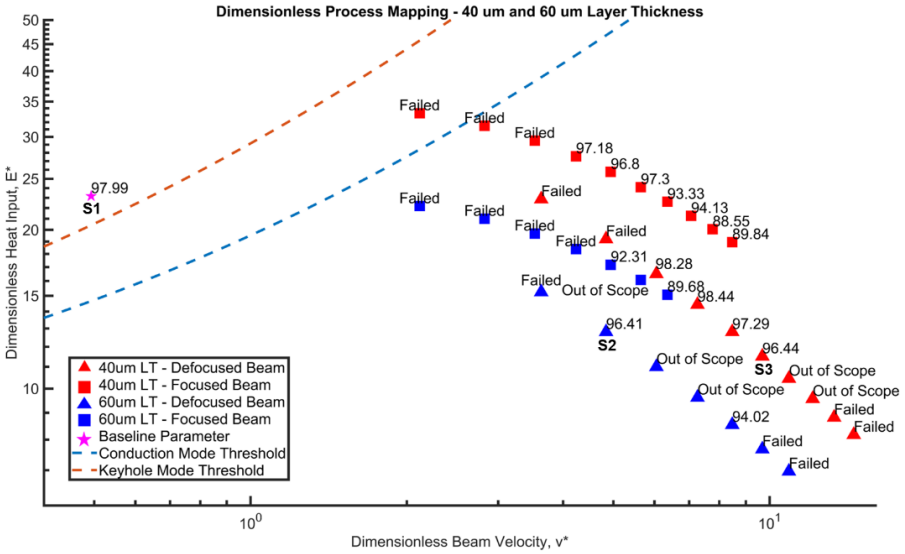

Figure 1. Dimensionless process map illustrating the effects of PD, LT, and beam focus on part density. Baseline parameters (pink star) are compared with improved conditions at LT = 60 µm (blue) and LT = 40 µm (red), using focused (squares), and defocused (triangles) beams. Density values (%) are annotated next to successfully printed samples. Dashed lines indicate the melting mode thresholds: conduction (lower line) and keyhole (upper line). Within each group, samples in the top left correspond to smaller PDs, while those toward the bottom right represent progressively larger PDs. S1-S3 indicate selected samples for further analysis.

The process parameters used to print the baseline sample (S1) were selected as a reference point for further refinement. The first set of adjustments involved varying the PD while keeping a constant LT of 60µm (blue square and triangle markers in Figure 1). The second modification focused on the effect of the laser beam diameter, in which a focused beam with a diameter of 70 µm (blue square markers in Figure 1) was compared to a defocused beam with a diameter of 120 µm (blue triangle markers in Figure 1). To further improve results, additional experiments were carried out using a reduced LT of 40 µm (red square and triangle markers in Figure 1). As with the previous set, PD and beam diameter were systematically varied while keeping the layer thickness constant. These new conditions are represented by red square markers (focused beam, 70 µm) and red triangle markers (defocused beam, 120 µm) in Figure 1.

The dimensionless process map revealed clear trends between process parameters and the density of the printed magnets. For both LTs, the samples from each set that achieved the highest densities tend to be the result of moderately small PDs

and the use of a wider defocused beam, suggesting that a balanced approach (high enough energy for full melting but diffuse enough to avoid defects) is most effective for this material. The use of a defocused beam likely contributed to a more uniform energy distribution, reducing peaks in energy density and thermal gradients. The effect of LT was also evaluated, and in general, the 40 µm group outperformed the 60 µm group in achievable density. This improved performance can be attributed to the reduced energy demand required to melt thinner layers. In contrast, thicker layers require a higher energy input to achieve comparable melting, increasing the risk of overheating and defect formation.

3.2. Thermal effects on the magnetic behaviour and defect formation

Three representative samples (S1, S2, and S3) were selected for detailed magnetic characterization and µXCT analysis. The magnetic characterization results (Figure 2a) revealed significant differences in remanence and coercivity. The baseline sample S1 (pink) had the lowest magnetic performance (B_r = 0.30 T, H_{ci} = 38.97 kA/m) despite achieving the highest density (97.99%). In contrast, S2 (blue) showed a substantial increase in coercivity and a comparable remanence (B_r = 0.29 T, H_{ci} = 610.82 kA/m), however, density slightly decreased (96.41%). S3 (red) achieved the best overall magnetic performance (B_r = 0.51 T, H_{ci} = 673.22 kA/m), despite a lower density (96.44%) than the baseline sample.

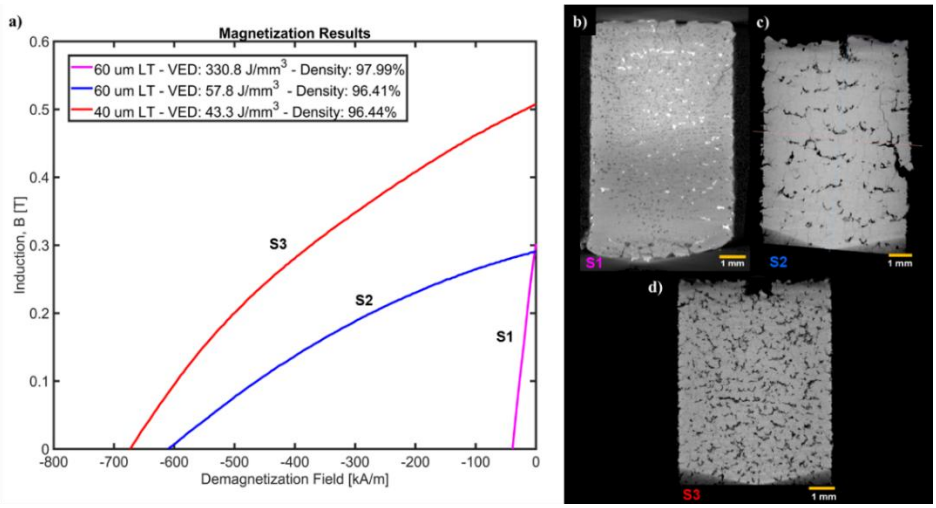

Figure 2. a) Magnetization results and corresponding µXCT images. a) shows colour-coded magnetization curves matching their respective µXCT cross sections (b-d). The sample printed with the baseline parameters and highest VED (S1) showed the lowest magnetic performance. In contrast, samples printed with lower VEDs (S2 & S3) exhibited a significantly better magnetic response.

Volumetric energy density (VED) was used to compare the effects of different process parameter combinations. S1, printed with the highest VED (330.8 J/mm^2), achieved the highest density, but the poorest magnetic performance. In contrast, S2 and S3, printed with much lower VEDs (57.8 and 43.3 J/mm^2), resulted in significantly better magnetic properties. Although in this study maximum VED yielded the highest density within the parameter window (S1), it should be noted that this is not a universal trend, as excessively high VED can also promote defect formation (e.g. keyholing and evaporation-induced porosity). Correspondingly, the excessive heat input likely promoted vaporization of Nd and B, essential for stabilizing $Nd_2Fe_{14}B$, the primary magnetic phase. In contrast, lower VEDs likely helped to preserve these elements and therefore the critical magnetic phases, resulting in higher coercivity and remanence despite the higher porosity. µXCT scans (Figure 2b-d) support these trends. S1 (Figure 2b) appeared structurally dense but exhibited microcracking and keyhole-type porosity (dark and bright regions) as predicted by the dimensionless process map (Figure 1). S2 (Figure 2c) displayed larger cracks and interconnected porosity, while S3 (Figure 2d) displayed finer, uniformly distributed pores and minimal cracking, consistent with more stable melt pool dynamics. These results demonstrate the strong dependence of microstructural evolution on the energy input. At high VEDs (S1), unstable melt pool dynamics and localized overheating promoted keyhole porosity. In contrast, lower VEDs (S2 and S3) led to a more uniform pore distribution and minimized overheating, however, the reduced energy input was insufficient for complete consolidation, leading to lack-of-fusion pores (Figure 2c and d). Despite the associated decrease in density, lower VEDs facilitated a more stable solidification pathway and better preservation of volatile elements, resulting in higher coercivity and remanence. Altogether, these findings emphasize that higher density alone does not guarantee better magnetic properties. Instead, careful process optimization to tailor the microstructure is essential not only for densification, but to minimize the elemental evaporation to preserve critical magnetic phases.

3.3. Demonstration of complex-shape printability

To demonstrate the applicability of the optimized parameters beyond simple cylindrical geometries, complex-shaped demonstrator parts (Figure 3a) were printed using the same conditions that yielded the best magnetic properties (LT = 40

µm and low VED). As shown in the magnified images (Figure 3b & c) the parts exhibit good dimensional accuracy, clear surface details, and minimal visible defects, confirming that the process window identified in this study is suitable for manufacturing structurally sound and magnetically functional components with intricate geometries.

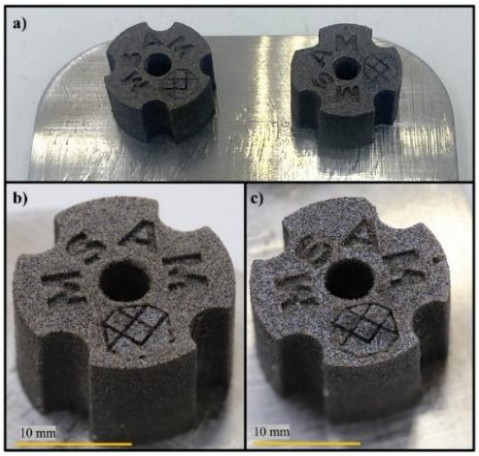

Figure 3. Optimized PBF-LB demonstrator parts. a) Complex magnets on the build plate, printed with two 40 µm LT recipes. b-c) Magnified views highlighting dimensional fidelity and surface quality with relative densities of 96.44 and 94.13%, respectively.

4. Conclusions

Systematic variation of PBF-LB process parameters revealed their effects on density and magnetic performance, while enabling the successful AM of NdFeB magnets with simple and complex geometries. The key findings are as follows:

1) Reducing the layer thickness from 60 µm to 40 µm consistently improved the final part quality and density.
2) Enhanced magnetic properties were associated with lower volumetric laser energy density during printing.
3) Notably, higher density did not necessarily correlate with an improved magnetic performance, highlighting the critical influence of the underlying microstructure and the preservation of critical magnetic phases.

Ongoing work aims to identify the optimal microstructure governing the magnetic performance of PBF-LB magnets.

5. Acknowledgments

The authors appreciate the funding support received from Greenage Materials, the Mitacs Accelerate Program grant #IT40655, and the support received from FedDev Ontario Regional Innovation Ecosystem grant #1016969. In addition, the authors would like to acknowledge the help of Jerry Ratthapakdee for his help with the PBF-LB prints and the motivation and support of the Multi-Scale Additive Manufacturing (MSAM) Lab at the University of Waterloo.

6. Conflicts of interest

The authors declare no known competing interests or relationships that may have influenced this work.

7. References

[1] Brown D, Ma B-M, Chen Z. Developments in the processing and properties of NdFeb-type permanent magnets. J Magn Magn Mater 2002;248:432–40.
[2] Paranthaman MP, Shafer CS, et al. Binder Jetting: A Novel NdFeB Bonded Magnet Fabrication Process. JOM 2016;68:1978–82.
[3] Li L, Tirado A, et al. A novel method combining additive manufacturing and alloy infiltration for NdFeB bonded magnet fabrication. J Magn Magn Mater 2017;438:163–7.
[4] Sridharan N, Cakmak E, et al. Rationalization of solidification mechanism of Nd–Fe–B magnets during laser directed-energy deposition. J Mater Sci 2018;53:8619–26.
[5] Sun X, Huang J, et al. FDM-based magnetically enhanced 3D printing of plastic materials. 2024 IEEE 1st Int. Workshop Future Intell. Technol. Young Res. FITYR, 2024, p. 91–96.
[6] Pigliaru L, Rinaldi M, et al. 3D printing of high performance polymer-bonded PEEK-NdFeB magnetic composite materials. Funct Compos Mater 2020;1:4.
[7] Lamarre J-M, Bernier F. Permanent Magnets Produced by Cold Spray Additive Manufacturing for Electric Engines. J Therm Spray Technol 2019;28:1709–17.
[8] Bernier F, Lamarre J-M, et al. Anisotropic Magnets Fabricated by Cold Spray Additive Manufacturing. J Jpn Soc Powder Powder Metall 2025;72:S219–26.
[9] Rong Chan Y, Seetharaman, et al. Advancing neodymium permanent magnets with laser powder bed fusion technology: a comprehensive review of process–structure–property relationship. Mater Adv 2024;5:8755–71.
[10] Patel S, Vlasea M. Melting modes in laser powder bed fusion. Materialia 2020;9:100591.
[11] Patel S, Chen H, et al. The influence of beam focus during laser powder bed fusion of a high reflectivity aluminium alloy — AlSi10Mg. Addit Manuf 2022;59:103112.
[12] Walls X, Lam R, et al. Influence of Melting Mode Process Mapping on the Properties of Additive Manufactured NdFeB Rare Earth Magnets using Laser Powder Bed Fusion. Under Preparation for submission.